Nuclear Engineering and Design 421 (2024) 113053

Contents lists available at ScienceDirect

Nuclear Engineering and Design

journal homepage: www.elsevier.com/locate/nucengdes

Measurement of the heat power generated by decay of fission products in fuel assemblies of the IEA-R1 research reactor

Adelk C. Prado *, Luís A.A. Terremoto, Pedro E. Umbehaun, Delvonei A. Andrade

Instituto de Pesquisas Energéticas e Nucleares, IPEN/CNEN-SP, Av. Lineu Prestes, 2242, CEP 05508-000, São Paulo, Brazil

ARTICLE INFO

Keywords:
Decay heat
Nuclear spent fuel
Fission products
Calorimetry

ABSTRACT

Fuel assemblies of the IEA-R1 research reactor were probed in calorimetric experiments. A special calorimeter was commissioned for that purpose. A theoretical model was proposed for the calorimeter. The fuel assemblies EC214, EC210 and EC207 were probed with cooling times ranging from 22 hours to 1043 days and declared U-235 burnup ratios ranging from 36 % to 45 %. Decay heat power was measured in the range of 4,1 W to 90 W, within ±5 % uncertainty. Because decay heat power is closely correlated to the actual inventory of fission products, the calorimeter was proven suited for enhancing non-destructive characterization of irradiated fuel assemblies.

1. Introduction

The IEA-R1 is an open pool research reactor which has been operational since 1957. Spent fuel characterization is an issue that tends to gain relevance as decommission becomes imminent and demand for spent fuel assembly transportation and storage is anticipated.

The inventory of fission products is of utmost importance for spent fuel characterization and is usually assessed by means of burnup calculation codes. Such calculations are often validated by means of fuel burnup verification, which is usually achieved through complex, expensive radiochemical analysis (International Atomic Energy Agency, 2009; Momotova et al., 2021; Roach et al., 2022). On the other hand, fuel assembly decay heat, which is closely correlated to the actual inventory of fission products (Tobias, 1980; Gauld, 2019), can be assessed through relatively inexpensive methods. Although intrinsically less accurate, non-destructive experimental evaluation of fuel assembly decay heat is perceived as a potential means toward the validation of fission products inventory calculations which is expected to be cost-effective.

In view of that, a batch of simple experiments were proposed in order to accurately assess the heat power generated by decay of fission products accumulated in irradiated fuel assemblies of the IEA-R1 reactor. A special fuel assembly calorimeter was commissioned for that purpose. The calorimeter is presented in this work, as well as the very first calorimetric experiments performed with its use.

2. Materials and methods

2.1. The IPEN fuel assembly calorimeter

The IPEN fuel assembly calorimeter features a submersible measurement vessel, a detachable lid and a movable control rack. The vessel is a 0,23 m diameter, 1,6 m high cylinder with hollow walls. Most of the vessel parts are made of machined high-density polyethylene. The measurement chamber is roughly 1 m high and is suited for regular IEA-R1-type fuel assemblies, which can be inserted through a 0,14 m diameter opening. The chamber features an embedded electric heater, which is used for calibration.

Heat flow sensors are embedded in the side walls of the vessel. The sensors are assembled in a 12x16 array to form a 0,31 m^2 12-sided prismatic heat sensitive surface, which roughly corresponds to 1/3 of the outer surface of the vessel. The heat flow sensors are 0,04 m x 0,04 m Bi_2Te_3 thermoelectric modules (Everredtronics Ltd, 2018).

A small water pump is embedded in the vessel lid. The pump is used to force water circulation throughout the chamber volume, thus improving temperature uniformity.

The control rack features a data acquisition system, an uninterruptible power unit and a PC-type computer. The calorimeter is operated via LabVIEW virtual instruments.

* Corresponding author.
E-mail address: acprado@ipen.br (A.C. Prado).

https://doi.org/10.1016/j.nucengdes.2024.113053
Received 10 November 2023; Received in revised form 15 February 2024; Accepted 22 February 2024
Available online 13 March 2024

2.2. Theoretical model for the calorimeter

As long as the vessel lid is in place, the measurement vessel can be regarded as a closed system, which has the reactor pool water as its surroundings (Fig. 1).

All the energy that enters the system comes either from the sample inside the chamber (decay heat from a fuel assembly), from the calibration heater or from the water circulation pump. Follows from the first law of thermodynamics that this energy adds to the internal energy of the system, by rising the average water temperature inside the chamber, until it eventually leaves the system, rejected to the cooler pool water, through the vessel walls. The energy balance of the system can be summarized as

$$S + H + P = dU/dt + R, \tag{1}$$

where S = decay heat power generated in the probed fuel assembly, H = power applied to the calibration heater, P = power applied to the water pump, U = internal energy of the system, R = heat power rejected through the vessel walls.

Assuming all the system internals are incompressible, an approximation may be taken:

$$S + H + P \cong CdT/dt + R, \tag{2}$$

where C = the equivalent heat capacity of the system and T = the mean temperature inside the measurement chamber.

Thermoelectric devices are used in the IPEN calorimeter as heat flux sensors, which is a consolidated practice in microcalorimetry (Wadsö, 1997). Thermoelectric devices have the distinctive property of generating a measurable voltage which is proportional to the rate of heat exchange through its sensitive surfaces (Nolas et al., 2013):

$$v \propto \dot{q}, \tag{3}$$

where $\dot{q}$ = the rate of heat exchange and v = the corresponding generated voltage.

Each side of Equation (3) can be summed over the full array of sensors installed in the measurement vessel walls, which leads to

$$V \propto \dot{Q}, \tag{4}$$

where V = the aggregate generated voltage and $\dot{Q}$ = the rate of aggregate heat exchange.

Due to the thermal isolation provided by the vessel walls, the heat flux sensors themselves constitute the path of least resistance for rejection of heat power R. Hence, most of the rejected power is conducted through the heat flux sensors, which makes R and Q closely correlated to each other. Now, follows from Equation (4) that, since R and Q are correlated, R is also correlated to V:

$$R \cong aV + b, \tag{5}$$

where a and b are defined as the calibration constants of the calorimeter.

Equation (5) can be used to rewrite Equation (2):

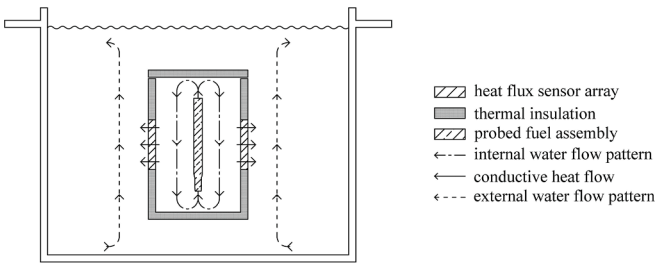

Fig. 1. Schematic representation of the calorimeter vessel while submerged in the IEA-R1 reactor pool.

$$S \cong aV + b + CdT/dt - H - P. \tag{6}$$

Now, since V, T, H and P can be easily measured and C can be estimated from design data, Equation (6) provides a means to assess the heat power S generated by a sample inside the chamber.

Equation (6) is derived from an approximation which relies on the fact that most of the heat R is rejected by means of conductive heat transfer (Equation (5). Actually, some convective heat exchange must be expected to take place as well, and even radiative heat exchange becomes significant as R approaches the operational power limit of the calorimeter (1 kW). Since both convective and radiative heat transfer have significant nonlinear dependence on the temperature differences that cause heat power R to be rejected, constants a and b on Equations (5) and (6) must be expected to vary among different intervals of R.

For the special case in which no power is generated and the system has reached a steady state, Equation (6) reduces to

$$a^{'}V + b^{'} = 0. \tag{7}$$

But since no power enters the system in this case, the principle of conservation of energy can be invoked to prove V must also be zero (otherwise electric power could be produced out of nothing), which leads to

$$b^{'} = 0. \tag{8}$$

Follows from Equations (7) and (8) that, as long as the total power entering the system is close enough to zero, Equation (6) can be further simplified:

$$S^{'} \cong a^{'}V = CdT/dt - H - P. \tag{9}$$

Equation (9) will be proven useful for probing dim heat sources, when S is close to the lower limit of the measurement range.

2.3. Probed fuel assemblies

IEA-R1 fuel assemblies EC214, EC210 and EC207 were probed in calorimetric experiments. Both fuel assemblies have U_3Si_2-Al dispersion fuel, with U density of 3,0 gcm^{-3}. EC214 has been part of the reactor core since October 2011, and its U-235 burnup was declared 37 % when the experiments were carried out. EC210 has been part of the core since June 2011, and its U-235 burnup was declared 43 % when the experiments were carried out. EC207 had been part of the core from January 2011 to December 2018, and its final U-235 burnup was declared 45 %.

The IEA-R1 DMPV-01 was also used in the experiments. Bearing no fissile material, the DMPV-01 is a dummy assembly which was devised for in-core flow distribution assessment (Torres et al., 2003). The DMPV-01 was kept inside the measurement chamber while calibration data were collected. This procedure was intended to ensure the reproduction of the water flow pattern that was expected during experiments with true fuel assemblies.

3. Results

The measurement vessel was installed in the reactor pool (Fig. 2). The control rack was installed in the reactor pool side.

3.1. Data acquisition

The electric calibration heater is connected in 4-wire mode: power is supplied through two wires while voltage is measured trough the other two. The 4-wire mode allows the measurement of the voltage over the heater itself, irrespective of the voltage drop over the cables through which the power is supplied. The voltage over the heater is sampled on one of the analog inputs of a 12-bit analog-to-digital converter (National Instruments DAQCard 6062E).

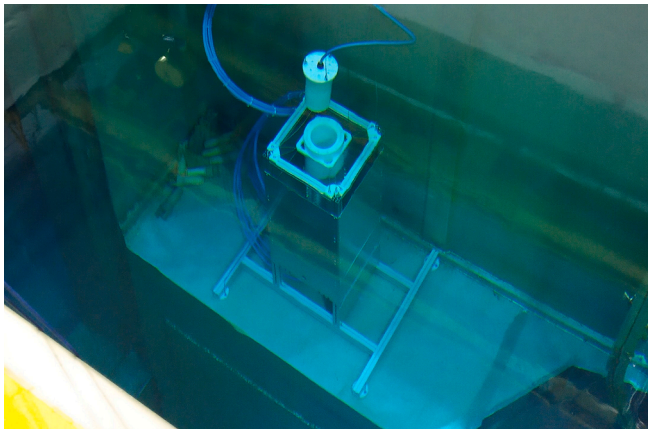

Fig. 2. The vessel of the IPEN fuel assembly calorimeter and the vessel lid, both submerged in the IEA-R1 reactor pool.

A precision shunt resistor (Vishay VCS301) is used in order to probe the current that flows through the heater driving circuit. The corresponding signal is sampled on another channel of the DAQCard 6062E.

The heater is driven by an alternative current (AC) power supply. The energy effectively transferred to the heater (H) is calculated for each period of 1 s. The calculation is performed by means of numerical integration of the product voltage·current over the corresponding sets of samples. The average power is calculated accordingly.

Sampling of both voltage and current relative to the water circulation pump are performed analogously to the sampling of voltage and current relative to the calibration heater. The pump is driven by a direct current (DC) power supply. The average power effectively transferred to the pump (P) is assumed as the product (average voltage)·(average current).

The analog channels are sampled at 30720 Hz, which is an integer multiple of the fundamental frequency of the local energy distribution lines (30720 Hz = 512·60 Hz). This is a good practice for reducing the effects of electromagnetic induced noise. The multiple 512 was chosen as high as possible, given the limitations of the analog-to-digital conversion hardware.

All analog channels used in voltage and current sampling were calibrated against a precision digital multimeter (Fluke 8846A).

Water temperature is measured by means of resistance temperature detectors (RTD). Excitation current and signal conditioning are provided by SCC-RTD01 modules (National Instruments). All channels used in temperature sampling were calibrated against a precision thermometric bridge (Automatic Systems F700).

Uncertainties on sampled voltage, current and temperature are mostly due to the offset and gain temperature coefficients of the analog-to-digital converter. This is due to the ambient temperature fluctuations at the pool side, where the data acquisition system was installed. Pool side temperature fluctuates between 18 °C and 31 °C, which is partly due to the mean temperature of the pool water, which peaks around 40 °C. Irregular operation of the local air conditioning system also contributed to the relatively high ambient temperature span at the reactor pool side.

The thermoelectric voltage V is sampled on the analog channels of a 16-bit analog-to-digital converter (National Instruments DAQCard AI 16XE 50). All analog channels were checked for offset errors. Absolute offset errors were found on the order of 10^{-4} V or less, which was assumed acceptable.

The calibration against a precision voltmeter was dismissed for the channels used in thermoelectric voltage sampling. Rather, those channels were calibrated against known heat sources, which is shown next.

3.2. In-pool calibration

As long as calibration is performed with no decay heat source ($S = 0$), follows from Equations (2) and (5) that

$$H + P - CdT/dt \cong R \cong aV + b. \tag{10}$$

With the vessel submerged in the IEA-R1 reactor pool, controlled power was applied to the embedded electric heater, and the thermoelectric voltage was measured for different levels of power in the range 0 ~ 100 W. Data shown in Fig. 3 were calculated from experimentally sampled H, P, dT/dt and V, which were averaged over 3600 s intervals. The equivalent heat capacity was calculated from design data, which led to $C = 90$ kJK^{-1}.

In view of Equation (10), a linear model was fitted to the data points, which produced the calibration constants (Fig. 3)

$$a = (21,55 \pm 0,06)\text{W/V and} \tag{11}$$

$$b = (0,4 \pm 0,2)\ \text{W}. \tag{12}$$

3.3. Measurement lagging time and lagging error

Data samples were taken while controlled power steps were applied to the calibration heater. A power step I of 200 W height and transition at $t = t_0$ is shown in Fig. 4, as well as the calorimeter response O and the calculated deviations. Notice that the normalized absolute deviations are reduced to 5 % or less, provided at least 1 h has passed since t_0. This was found typical when the calorimeter is operated in forced circulation mode ($P > 0$). Accordingly, the measurement lagging time τ relative to forced circulation mode was assumed not greater than 1 h.

The calorimeter was also probed for transient response in free circulation mode ($P = 0$), for which the measurement lagging time was found not greater than 2 h.

Relative to the actual power I shown in Fig. 4, the calorimeter response O is delayed in time, which is mostly due to the heat capacity C. In fact, at any given time t, $O(t)$ provides an estimate for the actual generated power $I(t')$, averaged over $(t–\tau) < t' < t$, within ±5 % error. What matters at the time t though is $I(t')$ averaged over $(t–\tau/2) < t' < (t + \tau/2)$, which must be assessed as $O(t + \tau/2)$. Now, provided O has a near-constant slope, the error due to lagging time can be approximated by

$$L \approx \bar{I}(t-\tau,t) - \bar{I}(t-\tau/2,t+\tau/2) \approx O(t) - O(t+\tau/2) \approx -\tau/2(dO/dt(t)), \tag{13}$$

where L is the error due to lagging time τ and $\bar{I}(t_1, t_2)$ is the average value of $I(t)$ over the time between t_1 and t_2.

Measurement lagging time is a cause of error when calorimetric experiments are carried out with time-dependent sources of power, such as irradiated fuel assemblies. Although Equation (13) is not reliable for power prediction, it will be useful when calculating the contribution of lagging error to the total uncertainty on S.

3.4. Decay heat power measurements

The EC214 was probed after 16 cooling hours. Decay power S was found by solving Equation (6) and is shown in Fig. 5, as well as the water pump power P and the internal energy variation CdT/dt. Notice that S falls as cooling time increases, which is in agreement with Wigner-Way analytical predictive model for decay heat after reactor shutdown (Lewis, 2008).

The EC214 decay heat power was found

$$S = (88 \pm 2)\text{W} - (3,70 \pm 0,05)(t/\text{hour} - 22)\text{W}, \tag{14}$$

where t is the cooling time in hours and $21 < t/\text{hour} < 23$.

The EC214 was also probed after 40 cooling hours, which resulted in

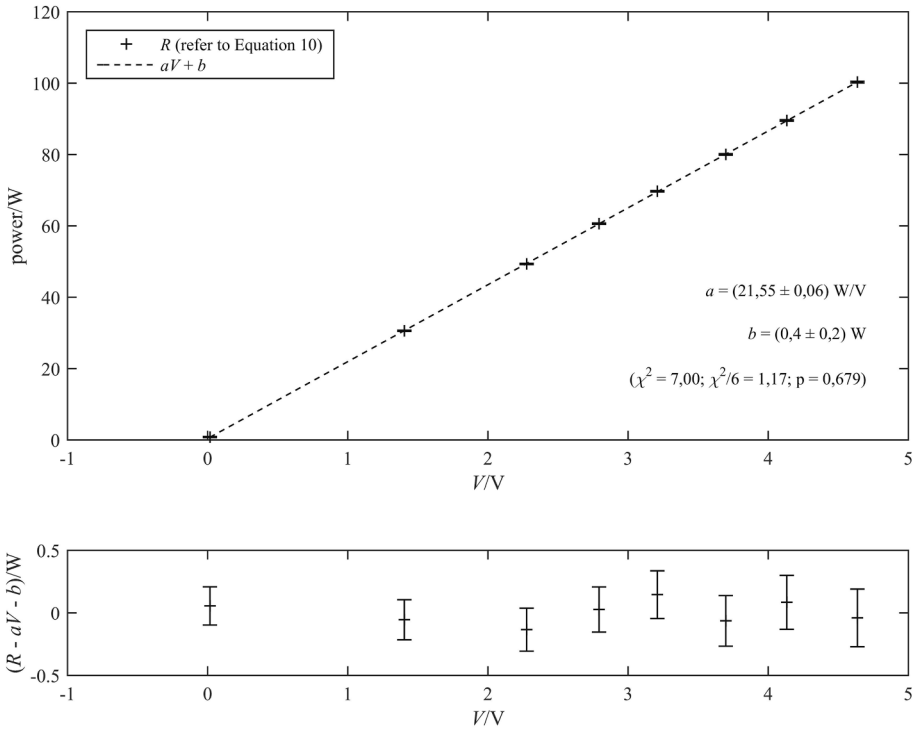

Fig. 3. Calibration data and fitting.

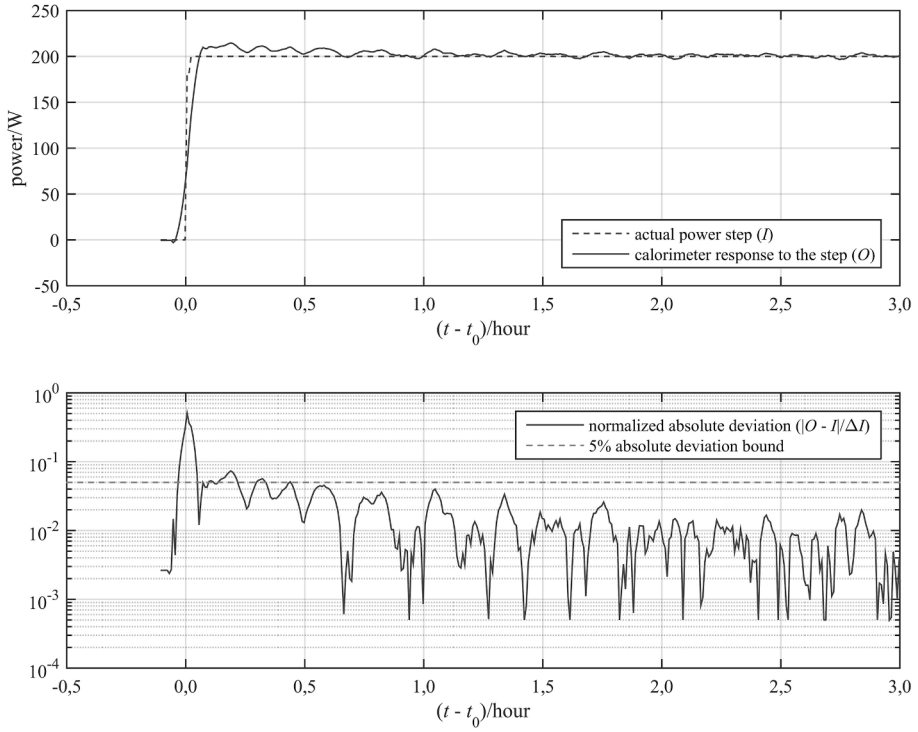

Fig. 4. Measurement lagging time in forced circulation mode.

$$S = (46 \pm 1)\text{W} - (0,90 \pm 0,04)(t/\text{hour} - 46)\text{W}, \quad (15)$$

where t is the cooling time in hours and $45 < t/\text{hour} < 47$.

The EC210 was probed after 40 cooling hours. In this instance the calorimeter was operated in natural circulation mode ($P = 0$). Decay power S is plotted in Fig. 6, as well as internal energy variation CdT/dt.

The EC210 decay heat power was thus found

$$S = (87 \pm 2)\text{W} - (1,56 \pm 0,05)(t/\text{hour} - 46)\text{W}, \quad (16)$$

where t is the cooling time in hours and $45 < t/\text{hour} < 47$.

The EC210 was also probed after 65 cooling hours, which resulted in

$$S = (63 \pm 1)\text{W} - (0,51 \pm 0,04)(t/\text{hour} - 72)\text{W}, \quad (17)$$

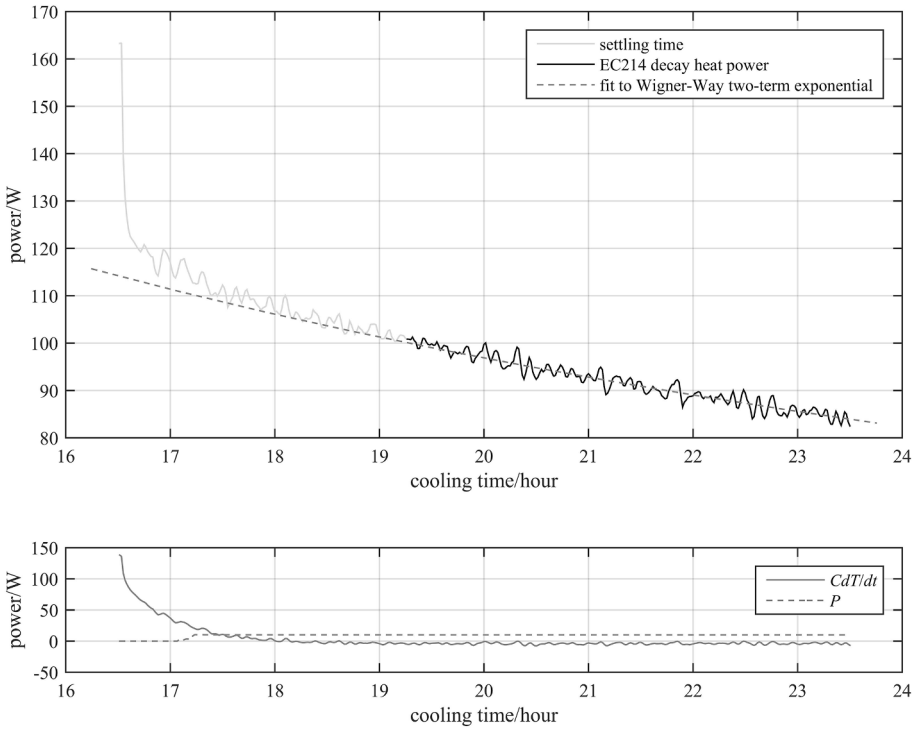

Fig. 5. Decay heat power from EC214 with cooling time around 22 h.

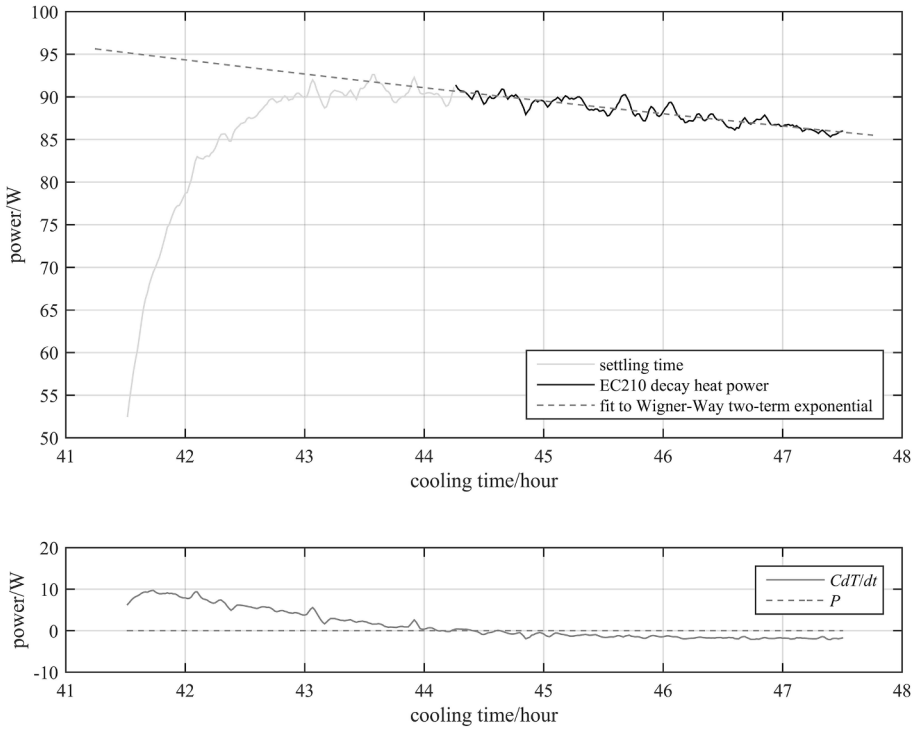

Fig. 6. Decay heat power from EC210 with cooling time around 46 h.

where t is the cooling time in hours and $71 < t/\text{hour} < 73$.

The EC214 was probed after 500 cooling hours. In this instance decay power S was averaged over 1800 s sampling intervals, which produced the results shown in Fig. 7.

The experimental data points shown in Fig. 7 were proved in good agreement with the Wigner-Way formula for total decay heat after reactor shutdown (Lewis, 2008). The average decay heat power was found

$$S = (11,2 \pm 0,4)\text{W} - (0,01 \pm 0,02)(t/\text{hour} - 500)\text{W}, \tag{18}$$

where t is the cooling time in hours and $475 < t/\text{hour} < 525$.

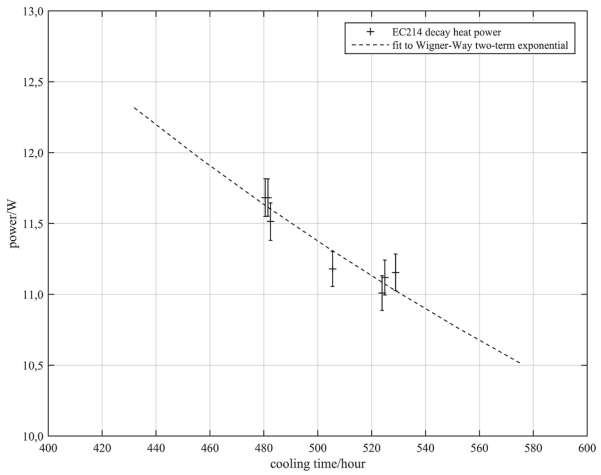

Fig. 7. Decay heat power from EC214 with cooling time around 500 h.

3.5. Concurrent calibration and decay heat measurement

The EC207 was probed after 1033 cooling days. Using calibration constants a and b (Equations (11) and (12)) the decay heat power was found (3,9 ± 0,4) W. In order to improve the measurement accuracy at this low power condition, a special procedure was devised by rearranging Equation (9) so that

$$H + P - CdT/dt \cong R' \cong a'V - S'. \tag{19}$$

No power was applied to the heater in this case ($H = 0$). The left-hand side of Equation (19) was calculated from samples of P and T. The results are plotted in Fig. 8 as a function of the measured thermoelectric voltage V. The plot refers to averaged values over 1800 s sampling intervals. In order to concurrently find the slope a' and the intercept ($-S'$), a linear model was fitted to the data points, which produced

$$S' = (4,1 \pm 0,1)\text{W}. \tag{20}$$

Including propagated uncertainties due to C, P and V, decay heat power in this case was found

$$S'' = (4,1 \pm 0,2)\text{W}. \tag{21}$$

The procedure leading to Equation (21) results in narrower uncertainty limits because it does not rely on a and b (Equations (11) and (12)), which by construction are wide range calibration constants (0 ~ 100 W).

4. Analysis and conclusions

4.1. Major contributions to uncertainty

The propagation of uncertainties is summarized in Table 1. All uncertainties were calculated to produce results with 95 % statistical confidence.

Measurement lagging time is propagated according to Equation (13). Negative lagging errors were calculated assuming maximum $\tau = 1$ h for forced circulation mode and maximum $\tau = 2$ h for free circulation mode. Positive lagging errors were all found null because minimum τ was assumed zero in both forced and free circulation modes. Lagging errors are major sources of uncertainty only for lower cooling times ($t < 500$ h).

Uncertainty on measurement of H is partly due to the calibration of the analog channels against a multimeter Fluke 8846A. It was found ±0,5% and is systematically propagated to S through the calibration constants.

Fitting uncertainties of the calibration constants a and b lead to interpolation error of ±0,2 W, which is also systematically propagated.

The heat capacity C (90 kJK^{-1}) was only determined within ±10 % uncertainty. Nevertheless, since data samples were only taken under near-steady conditions ($|dT/dt| < 10^{-6}$ Ks^{-1}), propagated uncertainties due to C were kept in the range ±0,4 W.

Uncertainty on measurement of P is also partly due to the calibration of the analog channels against a multimeter Fluke 8846A. It was found in the range ±0,03 W and does not apply when the calorimeter is operated in free circulation mode.

Deviations of $S(t)$ around its mean value are particularly clear in

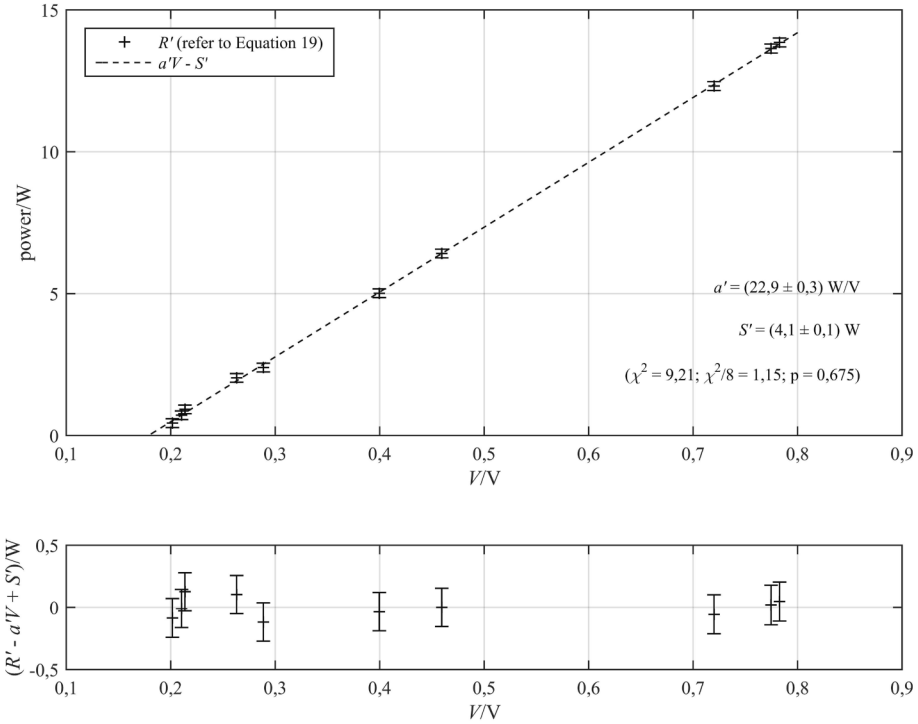

Fig. 8. Concurrent calibration and decay heat measurement applied to the EC207.

Table 1
Uncertainties impacting the assessment of decay heat power S in each studied case (all uncertainty limits presented in the table correspond to 95 % statistical confidence intervals).

			EC214/	EC214/	EC210/	EC210/	EC214/	EC207/
Source	Propagation	Unit	21 h ~ 23 h	45 h ~ 47 h	45 h ~ 47 h	71 h ~ 73 h	500 h	1040 d
S lag time	Systematic	W	[−2;0]	[−0,5;0]	[−2;0]	[−0,5;0]	[−0,01;0]	–
H	Systematic	W	±0,4	±0,2	±0,4	±0,3	±0,06	–
C	Systematic	W	±0,4	±0,2	±0,2	±0,2	±0,05	±0,05
a, b	Systematic	W	±0,2	±0,2	±0,2	±0,2	±0,2	–
P	Systematic	W	±0,03	±0,03	–	–	±0,01	±0,01
V	Statistical	W	±0,04	±0,03	±0,03	±0,02	±0,03	±0,01
S' fitting	Statistical	W	–	–	–	–	–	±0,1
Total uncertainty		W	[−3;1]	[−1;0,7]	[−3;0,8]	[−1;0,7]	±0,4	±0,2
Relative uncertainty			[−3 %;1 %]	[−3 %;2 %]	[−3 %;1 %]	[−2 %;1 %]	±4 %	±5 %

Figs. 5 and 6. These deviations are random, and cannot be correlated to V, T, H or P. Such deviations were attributed to unaccounted fluctuations on dU/dt, which result from the approximation assumed in Equation (2). Indeed, when computing Equation (2), T is taken as the average of two indications of temperature, one for the bottom of the measurement chamber and one for the top. Since T is only an approximation to the actual mean temperature of the system, CdT/dt must be expected to deviate from the actual dU/dt.

Opposite to EC214, EC210 was probed in free circulation mode. Total uncertainty of decay heat power found in the latter case is similar to that found in the former. This similarity was taken as an indication that the measurement accuracy is not significantly affected by the water flow pattern inside the measurement chamber.

4.2. Minor contributions to uncertainty

In order to avoid water pressure buildup inside the measurement chamber, a small gap is left between the lid flange and the vessel lid seat. When a heat source is probed, as the water temperature rises inside the chamber, a small amount of water leaks to the reactor pool, carrying some energy in the process:

$$dU/dt = udm/dt = u\rho_0 dV/dt = u\rho_0 V_0 \beta dV/dt, \tag{22}$$

where u = specific internal energy of water at local temperature and pressure, dm/dt = mass leakage rate, ρ_0 = initial water density, V_0 = volume occupied by water in the measurement chamber, β = volumetric temperature coefficient of water.

Local temperature T is kept below 60 °C, $V_0 = 0{,}02\ m^3$, $2{\cdot}10^{-4}\ K^{-1} < \beta < 5{\cdot}10^{-4}\ K^{-1}$ and $u \leq 250\ kJkg^{-1}$. Hence, provided all samples are taken while dT/dt is not greater than $10^{-6}\ Ks^{-1}$, Equation (22) can be used to prove that $dU/dt < 3{\cdot}10^{-3}$ W. This power leakage was assumed small enough to be disregarded.

The calibration was performed with the dummy assembly DMPV-01 inside the measurement chamber. Effects on equivalent heat capacity C due to replacing DMPV-01 with EC214, EC210 and EC207 were also disregarded.

4.3. Effect of gamma radiation over calibration constants

The decay heat power from EC207 was evaluated with use of constants a and b, which resulted in (3,9 ± 0,4) W. It was also evaluated with use of constants a' and b', which resulted in (4,1 ± 0,2) W. The former result derives from a calibration procedure which was carried out while no significant gamma-ray source was inside the measurement chamber (Section 3.2). The latter derives only from experiments carried out while the EC207 (which is a very high intensity gamma-ray source) was inside the chamber (Section 3.5). Because both results are overlapped, the effect of gamma-ray exposition on the properties of the heat flux sensors was assumed not significant. Accordingly, the use of the calibration constants a and b was assumed valid under the conditions reported throughout this work.

4.4. Escape of fuel assembly-originated gamma radiation

The spent fuel decay heat is partly due to the emission of gamma radiation as the accumulated fission and activation products decay (Tobias, 1980). Since gamma radiation is remarkably capable of penetrating matter and since true calorimetric vessels are subject to engineering constraints regarding their weight and volume, a true vessel would hardly be massive enough to completely shield the spent fuel-originated gamma radiation. Instead, it is likely that some radiation passes through the vessel boundaries, eventually depositing its energy in the near surroundings. In fact, the energy associated to the radiation escaping the vessel is a part of the spent fuel decay heat that cannot be measured by means of calorimetry, and must therefore be assessed separately.

The escape of gamma radiation has been investigated in previous calorimetric experiments regarding spent fuel assemblies from light water reactors (Sturek and Agrenius, 2006; Strickler and Doman, 1982; Strickler and Eger, 1981). In order to estimate the gamma escape during experiments with the GE-Morris device, gamma-ray countings were taken around the test vessel while a spent fuel assembly was inside it. In order to estimate the gamma escape during experiments with the Clab device, five movable gamma-ray detectors were used to scan the space around the test vessel. In both cases, gamma-ray countings were combined with proper geometrical models to produce estimates of the overall escape of gamma radiation and its corresponding energy. For the GE-Morris device, the gamma escape-related loss was estimated in the order of 2,5 % relative to the total decay heat power. For the Clab device, the losses were estimated for each probed fuel assembly, ranging between 2 % and 3 % relative to the total decay heat power. Although not negligible, gamma escape-related losses are only a minor contribution to the total decay heat power.

Notice that gamma probing methods are particularly sensitive to the geometry of both the fuel assembly and the detecting apparatus, in a way that avoiding bias requires very accurate and challenging modeling (Terremoto et al., 2000). As far as it concerns the assessment of decay heat, this sensitiveness at least partly explains why gamma probing has in fact been applied as accessory to the calorimetry, and not otherwise (Sturek and Agrenius, 2006; Strickler and Doman, 1982).

Regarding the IPEN calorimeter, up to this point no resources are in place for collecting experimental data on the escape of gamma radiation. In principle, the gamma escape could alternatively be derived from the theoretical fuel burnup, by means of a straightforward calculation. However, since the gamma escape is linked to the total decay heat, it is itself intended to enable the validation of the available fuel burnup reports, and such calculation would only lead to a circular reference. The assessment of the gamma escape was thus left for future developments. Indeed, resources are already secured to commission an upgrade that will allow the gamma-ray spectral analysis to be performed concurrently with the future calorimetric experiments, and a rugged gamma-ray spectrometer is currently being developed for that purpose.

4.5. Conclusions

The IPEN fuel assembly calorimeter was successfully installed in the IEA-R1 reactor pool. A simple theoretical model was proposed. The measurable output variable was proven closely correlated to the power generation inside the measurement chamber. An accurate measurement scale was found by means of carefully conducted calibration.

Calorimetric experiments were carried out with IEA-R1 irradiated fuel assemblies EC214, EC210 and EC207, with cooling times ranging from 22 hours to 1043 days, and declared U-235 burnup ratios ranging from 36 % to 45 %. Decay heat power was measured in the range of 4,1 W to 90 W, within ± 5 % uncertainty (with 95 % statistical confidence).

The calorimetric results were found accurate enough to enable future validation of decay heat power assessments derived from theoretical burnup calculations. More importantly, since decay heat power is closely correlated to the actual inventory of fission products, the calorimetric results could potentially be used to validate declared burnup reports without recurring to radiochemical methods. In view of that, the IPEN fuel assembly calorimeter was proven an affordable means for enhancing non-destructive characterization of irradiated fuel assemblies.

CRediT authorship contribution statement

Adelk C. Prado: Conceptualization, Methodology, Investigation, Software, Data curation, Writing – original draft, Writing – review & editing, Visualization. **Luís A.A. Terremoto:** Writing – review & editing. **Pedro E. Umbehaun:** Resources, Writing – review & editing. **Delvonei A. Andrade:** Supervision, Funding acquisition, Writing – review & editing.

Declaration of competing interest

The authors declare that they have no known competing financial interests or personal relationships that could have appeared to influence the work reported in this paper.

Data availability

Data will be made available on request.

Acknowledgements

The IPEN fuel assembly calorimeter was developed with financial support of the São Paulo Research Foundation (FAPESP), by means of the grant #2017/00634-0, and has been kept operational with resources secured by means of the grant #2021/06088-3. Infrastructural support was provided by the Nuclear Engineering Research Center at the IPEN/CNEN-SP.

References

Everredtronics Ltd, "Thermoelectric Module: TEC1-12706T125," Shanghai, [2018].
Gauld, I., 2019. Data Compilation and Analysis of Fission Product Decay Heat Experiments. International Atomic Energy Agency, Vienna.
International Atomic Energy Agency. 2009. "Post-Irradiation Examination and In-Pile Measurement Techniques for Water Reactor Fuels," Vienna.
Lewis, E.E., 2008. Fundamentals of Nuclear Reactor Physics. Academic Press, Burlington.
Momotova, V.N., Erina, E.A., Volkova, A.Y., Kupriyanova, V.N., 2021. Post-radiation radiochemical analysis of spent nuclear fuel from VVER-440 reactor. Radiochemistry 63 (2), 197–208.
Nolas, G.S., Sharp, J., Goldsmid, H.J., 2013. Thermoelectrics: Basic Principles and New Materials Developments, vol. 45. Springer Science & Business Media, Berlin.
Roach, B.D., Rogers, K.T., Zirakparvar, N.A., Delashmitt, J.S., Metzger, S.C., Manard, B. T., Keever, T.J., Giaquinto, J.M., Hexel, C., 2022. The need for speed – burnup determination of spent nuclear fuel. Talanta Open (6).
Strickler, H.R., Doman, J.W. 1982. "In-plant Test Measurement for Spent Fuel Storage at Morris Operation: Vol 3, Fuel Bundle Heat Generation Rates," San Jose.
Strickler, H.R., Eger, K.J. 1981. "In-plant Test Measurement for Spent Fuel Storage at Morris Operation: Vol 2, Fuel Bundle Radiation Levels," San Jose.
Sturek, F., Agrenius, L. 2006. "Part 1: Clab - Measurements of decay heat in spent nuclear fuel assemblies," in *Measurements of decay heat in spent nuclear fuel at the Swedish interim storage facility, Clab*, Stockholm.
Terremoto, L.A.A., Zeituni, C.A., Perrotta, J.A., Silva, J.E.R., 2000. Gamma-ray spectroscopy on irradiated MTR fuel elements. Nucl. Inst. Methods Phys. Res. A 450, 495–514.
Tobias, A., 1980. Decay heat. Prog. Nucl. Energy (5).
Torres, W.M., Umbehaun, P.E., Andrade, D.A., Souza, J.A. 2003. "A MTR fuel element flow distribution measurement preliminary results," in *25. international meeting on Reduced Enrichment for Research and Test Reactors (RERTR)*, Chicago, IL (United States).
Wadsö, I., 1997. Trends in isothermal microcalorimetry. Chem. Soc. Rev. 26, 79–86.